ACS OMEGA

Article

http://pubs.acs.org/journal/acsodf

Antimicrobial Properties of Copper-Doped ZnO Coatings under Darkness and White Light Illumination

Iman A. Hassan,[†] Sanjayan Sathasivam,[†] Sean P. Nair,[‡] and Claire J. Carmalt*,[†]

[†]Materials Chemistry Centre, Department of Chemistry, University College London, 20 Gordon Street, London WC1H 0AJ, U.K.
[‡]Department of Microbial Diseases, UCL Eastman Dental Institute, 256 Gray's Inn Road, London WC1X 8LD, U.K.

Supporting Information

ABSTRACT: We report the first antimicrobial study of transparent and robust Cu-doped ZnO coatings that displayed potent antimicrobial activity that resulted in bacterial (*Escherichia coli*) reduction below detection limits within 6 h of illumination via a white light source that is found in hospital environments. The same bacterial reduction rate was observed even under darkness for 4.0 atom % Cu-doped ZnO films thus providing an efficient 24 h disinfection. All films were produced via a novel, inexpensive, and easily scalable route and were also thoroughly analyzed for their material properties.

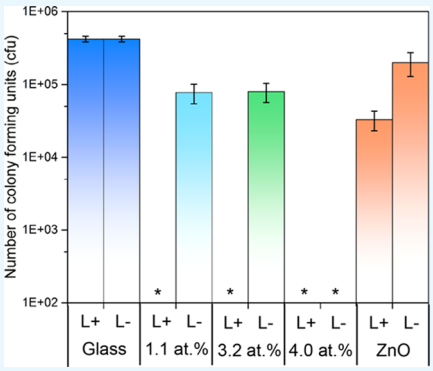

INTRODUCTION

Nosocomial infections are a major concern for hospitals and healthcare institutions globally.[1−3] Many of these infections are caused by multidrug-resistant strains of bacteria. If current trends persist, by 2050 antimicrobial drug resistance would lead to a loss of 10 million lives every year, with a reduction in the world gross domestic product of 2−3.5%, which translates to a cost of up to U.S. $100 trillion.[4,5] In hospital environments, which are the epicenter of a majority of these antimicrobial drug-resistant infections, 80% of infections are due to contaminated touch surfaces.[6−8] Disinfection of such surfaces is key to the fight against spread of antimicrobial bacteria.

Antimicrobial surfaces and coatings are widely used and usually consist of metal, metal oxides, or polymers doped with organic antibacterial compounds, such as methylene blue.[9−11] These coatings, when applied to high-contact touch surfaces in healthcare environments, are proving to be effective in the fight against hospital-acquired infections.

Zinc oxide is an inexpensive semiconducting material extensively used in the optoelectronic industry due to its wide band gap (3.3 eV at room temperature) and high electrical conductivity. Recently, it has found use as an antimicrobial agent and has seen application in the lining of food packaging to reduce spoilage.[12] The mechanism for the activity is complex and not fully understood, but it is thought to be through various paths, including the uptake of Zn^{2+} ions (released into the surrounding environment from the metal oxide surface) into cells. Zn^{2+} is an essential ion for many microorganisms due to its involvement in various cellular reactions, but at concentrations above 10^{-7} mol L^{-1} it becomes cytotoxic.[13−16] Another process is that it induces the formation of powerful oxidizing agents (such as hydrogen peroxide) within bacteria cells that can cause cell damage.[12] Further still, another action of antimicrobial activity of ZnO arises from its photosensitive properties. Upon irradiation by UV light with energy above 3.3 eV (sunlight and fluorescent light sources commonly found indoors emit light ca. 4% in the UV wavelengths, and some of this UV light will have energy above 3.3 eV), ZnO oxidizes and reduces water and oxygen (respectively) to produce reactive oxygen species (ROS).[12,17] These species can then cause damage to an organism's cell membrane, DNA, and protein through Fenton type reactions, which result in cell death.[18−23] Some believe this oxidative stress to be the primary mode of antibacterial activity of most bactericidal metal oxides.[24−27]

Copper, a well-known antimicrobial agent, is thought to show action against bacterium via Fenton type reactions.[28−32] Although a powerful and effective antimicrobial agent, copper is expensive and so can have high costs when required to coat high-contact surfaces that often have large areas. Furthermore, unlike ZnO that is transparent, in the thin-film form, Cu, Cu_2O, and CuO are not transparent but either opaque or colored. This can lead to esthetic issues when it comes to real world, nonlaboratory applications.

However, the use of copper as a dopant in a ZnO matrix may potentially circumvent the two aforementioned issues while enhancing the antimicrobial properties of ZnO. The use of Cu-doped ZnO would allow the films to remain transparent in the visible spectrum and provide a cheap (as only a small quantity of Cu is used) and mechanically robust solution while allowing attack of the bacterium using both Cu and Zn.

Received: June 9, 2017
Accepted: July 27, 2017
Published: August 16, 2017

DOI: 10.1021/acsomega.7b00759
ACS Omega 2017, 2, 4556−4562

In this article, we report for the first time, the antimicrobial activity of Cu-doped ZnO thin films. Although Cu-doped ZnO thin films have been reported before, their functional testing has been limited to applications, such as photocatalysis, ferromagnetics, and optoelectronics. To the best of our knowledge, no previous papers have examined the antimicrobial properties of Cu-doped ZnO in the thin-film form. Cu-doped ZnO has been investigated as an antimicrobial agent in the nanoparticulate and bulk powder variant against both Gram-negative and Gram-positive bacteria.[33] Although nanoparticulate ZnOs (and metals/metal oxides in general) show superior activity against bacteria compared with bulk powders or thin films due to the larger surface area (and hence higher contact with the bacteria), they are difficult to handle in nonlaboratory situations when not immobilized. When immobilized in, for example, polymers, they evidently lose some of their active surface area and thus their efficiency advantage. Thin films of ZnO are easy to handle and hard wearing, with almost no hazards to human health that are associated with loose nanoparticles.

Also, in this article, we show the novel use of aerosol-assisted chemical vapor deposition (AACVD) for the synthesis of the Cu-doped films. AACVD is a simple solution-based atmospheric pressure film growth technique that allows for easy scale up. In AACVD, the precursors need not be volatile, as they are simply dissolved in a suitable solvent and transferred to the deposition chamber as an aerosol mist via a carrier gas (see the Supporting Information).[34,35] Films produced via AACVD are of high quality and have been used in many applications.[36−39] The pure and Cu-doped films produced were tested for their material properties and tested against *Escherichia coli* for their antimicrobial functionality under both illuminated and dark conditions. The results showed potent antibacterial activity under both conditions.

RESULTS AND DISCUSSION

Pure and Cu-doped thin films of ZnO were deposited on glass substrates from methanol solutions of $Zn(OAc)_2{\cdot}2H_2O$ and differing molar concentrations of $Cu(OAc)_2{\cdot}H_2O$ at 350 °C using AACVD on glass substrates. The films were highly transparent in the visible region with a slight green coloration only at high (4.0 atom %) Cu dopant concentrations (see the Supporting Information). The films were also well adhered to the substrate, passing the Scotch tape and scratch tests involving pencils of various hardness.[40] Films were also stable when exposed to solvents such as methanol, toluene, and water. Only weak acid was able to remove the coatings from the substrates.

Material Characterization. Powder X-ray diffraction (PXRD) showed the films to be phase pure ZnO in the Wurtzite crystal structure (Figure 1a). Peaks at 31.9, 34.8, 36.7, 48.0, 57.2, and 63.5° 2θ values corresponding to (100), (002), (101), (102), (110), and (103) reflections, respectively, were observed. The broad nature of the peaks suggests the films have poor crystallinity, primarily due to the relatively low deposition temperature. Interestingly, the 4% Cu-doped sample was relatively higher in crystallinity as evident from the narrower nature of the peaks. Furthermore, for this film, the peak positions were shifted to higher 2θ values, indicating a possible contraction of the ZnO unit cell.

UV−vis measurements were carried out on the pure and Cu-doped ZnO films to obtain transmittance and reflectance data (Figure 1b). All films had a high transmittance in the visible and

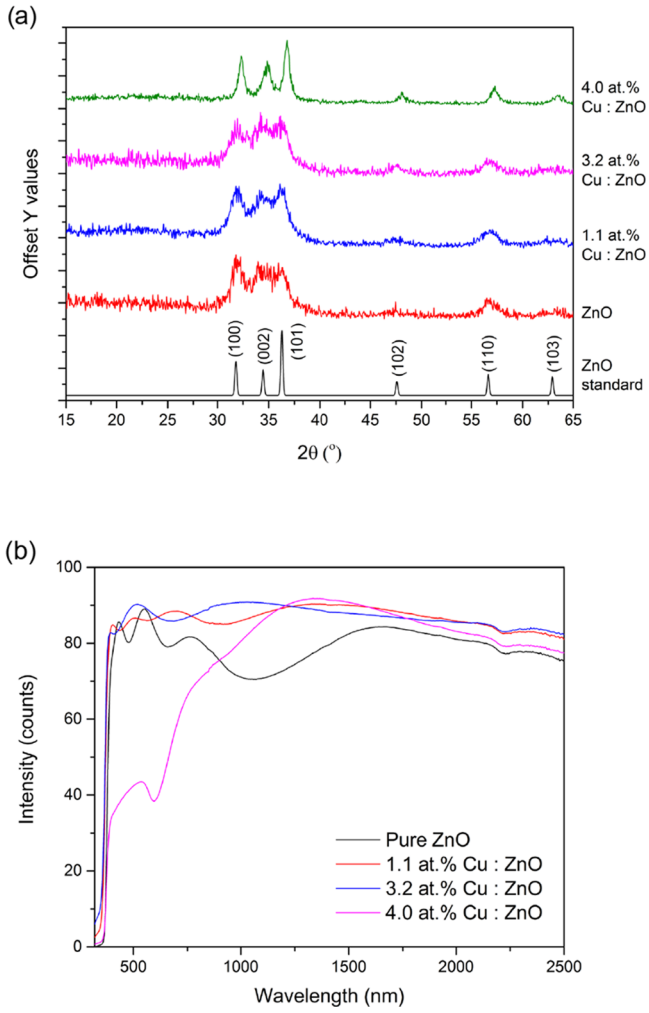

Figure 1. (a) PXRD and (b) UV−vis spectra of the AACVD-deposited ZnO and Cu-doped ZnO films on glass substrates.

near-IR region with a sharp absorption edge in the UV. With increasing Cu concentration, there was a decrease in transmittance. At 4.0 atom % Cu loading, the films showed a broad absorption peak at ca. 590 nm, leading to a green film.

The optical band gap was calculated for all films by applying the Tauc method to the UV−vis data, which showed no significant change in the band gap (3.3 eV) at the Cu doping levels carried out in this study. The reduction of the ZnO band gap when doping has only been achieved at high doping concentrations in the literature.[33] This is what was observed in this study too (data not shown); however, at these concentrations the films have a dark green/black coloration, which is not ideal esthetically as coatings on, for example, door handles and keyboards for antimicrobial applications.

The microstructure of the films was studied using a scanning electron microscope (SEM) (Figure 2). The pure ZnO film appears to have a faceted microstructure not unlike previously deposited ZnO films via AACVD.[41,42] Upon doping, especially at the higher Cu concentration regime, 3.2 and 4.0 atom % Cu, the morphology changes to a more globular structure consisting of semicircular domes. The size of these domes, in general, increases with increasing Cu concentration. For the 1.1 atom % Cu/ZnO film, the diameter of the domes was between a range of 50 and 100 nm, whereas for the 3.2 and 4.0 atom % films, the

DOI: 10.1021/acsomega.7b00759
ACS Omega 2017, 2, 4556−4562

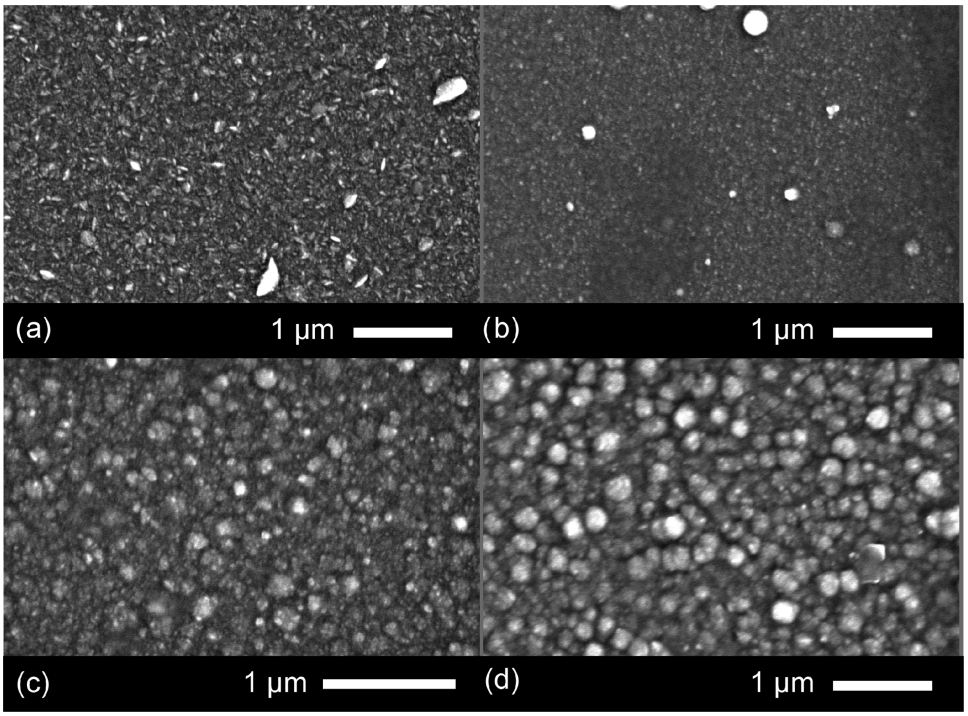

Figure 2. SEM images for (a) pure ZnO and (b) 1.1, (c) 3.2, and (d) 4.0 atom % Cu-doped films grown via AACVD at 350 °C.

range was between 100 and 600 nm. Overall, the films appear very compact and uniform, with no cracks, voids, or pinholes.

The films were also analyzed using energy dispersive X-ray spectroscopy (EDS) to probe the elemental composition (see the Supporting Information). It showed the pure and doped ZnO films to be free of any contaminants. The doped samples showed an increase in Cu concentration with increasing AACVD precursor concentration. Films made using 2, 4, and 8 mol % of $Cu(OAc)_2{\cdot}H_2O$ relative to $Zn(OAc)_2{\cdot}2H_2O$ showed 1.1, 3.2, and 4.0 atom % Cu compared with Zn in the films, respectively.

X-ray photoelectron spectroscopy (XPS) was carried out on the pure and Cu-doped ZnO films to determine the oxidation state and chemical composition at the surface (Figure 3). The core-level Zn 2p spectra showed peaks at 1021.5 eV for the $2p_{3/2}$ transition matching Zn in the +2 oxidation state, as expected and concurring with the literature examples (Figure 3a). The Cu 2p spectra showed a high signal to noise ratio due to the low dopant concentration (Figure 3b), but there is a single $2p_{3/2}$ peak at 933.0 eV suggesting the presence of Cu in the 0 and/or +1 oxidation states. It is difficult to differentiate between these two oxidation states of Cu from the XPS 2p transition alone due to heavy peak overlap.[43,44] Because of the lack of a satellite peak around 940 eV that is normally associated with Cu^{2+}, it can be concluded that there is none or very little Cu^{2+} present on the film surface. The ratio of Cu to Zn at the surface of the films, as observed from the XPS peak area analysis, increases with increasing dopant concentration and follows the trend that was seen from EDX results (a bulk analysis technique).

Valence band XPS of the films can be separated and discussed into two distinct features (Figure 4c,d). First, the peak at 10 eV can be assigned to the Zn 3d transition, whereas the second part between 7.5 and 0 eV, consisting of a broad hump that has some fine structure (when magnified), is comprised of two peaks at 6.5 and 4 eV. The small peak at 6.5 eV is made up of Zn 4s and O 2p mixing contributions, and the peak at 6.5 eV is made up of only O 2p contributions.[45] The position of the valence band maxima with respect to the Fermi level, determined via a simple linear extrapolation of the leading edge, is 2.5 eV for the 4.0 atom % Cu-doped ZnO film.

Antimicrobial Testing. The antimicrobial activity of the undoped and Cu-doped ZnO films deposited on microscope glass slides were determined using *E. coli*, a Gram-negative bacterium that is commonly found in hospital environments (Figure 4). Samples were cut into 1 × 1 cm^2 sections and were covered with 25 μL of bacterial suspension containing approximately 10^5 cfu. For each experiment, a set of samples were illuminated with a white light source (28 W), emitting an average light intensity of 3750 lx, at a distance of 30 cm from the sample. In all experiments, a control sample set was maintained in parallel and was stored under dark conditions for the same exposure times. The fluorescent lamp used emits light across the visible region of the spectrum, similar to those commonly found in U.K. hospitals. After incubation for set times, bacteria were recovered from the samples and the number of viable bacteria remaining was determined. The results demonstrate that the films indeed have antimicrobial activity against *E. coli*. Each bar represents the $\log_{10}$ of the mean number of viable bacteria from the two experiments carried out at different occasions, and error bars represent the calculated standard error.

After 3 h of exposure (Figure 4a), all of the films had a higher activity in the light (L+) rather than the dark (L−), except for the 4.0 atom % Cu-doped ZnO film that had the same reduction in bacterial numbers for both conditions (1.3 $\log_{10}$). After 6 h of exposure (Figure 4b), all Cu-doped ZnO films have significant reduction ($P < 0.01$) in the number of viable bacteria to below the limit of detection in the light. In darkness, there was only a small reduction in the counts for both 1.1 and 3.2 atom % Cu-doped films. After 18 h of exposure (Figure 4c), all samples (apart from pure ZnO in darkness) were able to impart

DOI: 10.1021/acsomega.7b00759
ACS Omega 2017, 2, 4556−4562

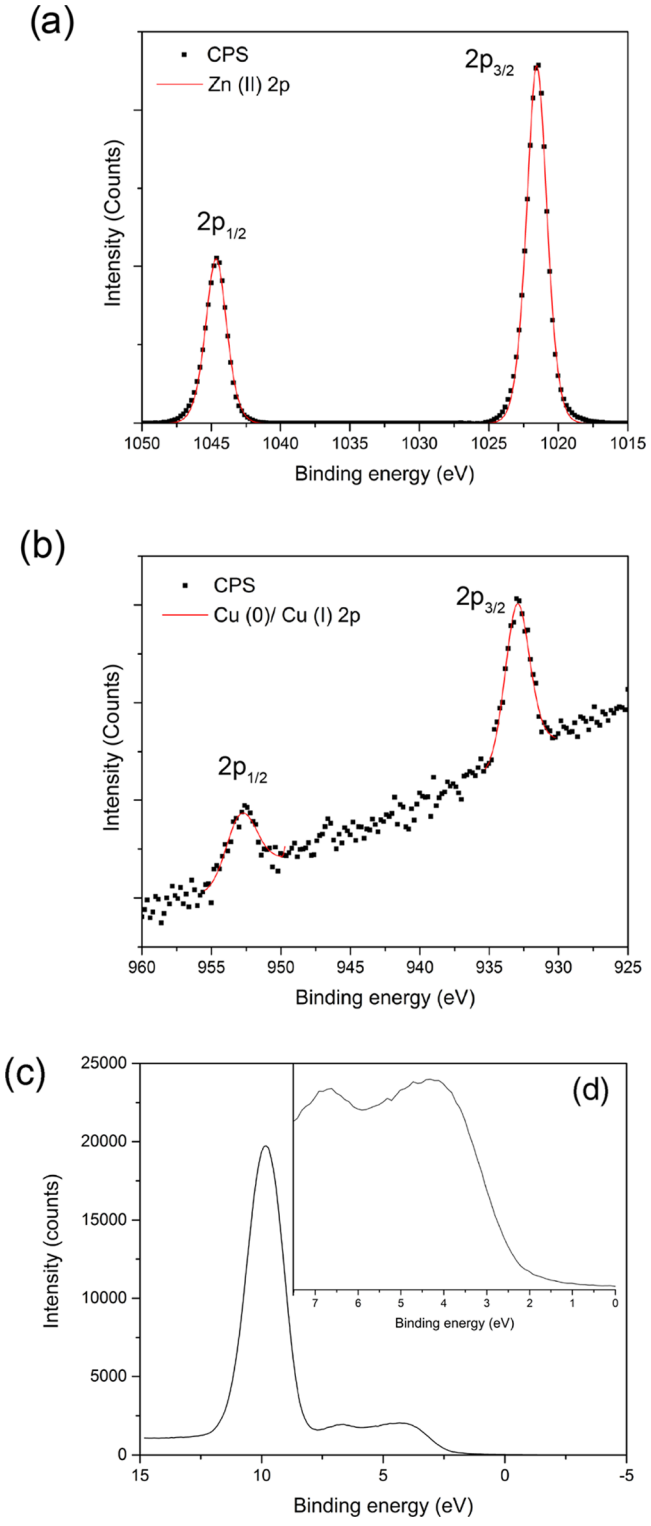

Figure 3. Typical core-level XPS spectra for the Cu-doped ZnO films grown via AACVD at 350 °C consisting of (a) Zn 2p transitions composed of a $2p_{3/2}$ peak at 1021.5 eV corresponding to Zn in the +2 oxidation. (b) Cu 2p spectrum made up of a single symmetrical peak at 933.0 eV in the $2p_{3/2}$ region matching Cu(0)/Cu(I). (c) Valence band XPS spectrum with a magnified inset (d) for the 0−7.5 eV region for the 4.0 atom % Cu-doped ZnO sample.

a reduction in the number of viable bacteria to below the detection limits ($P < 0.01$).

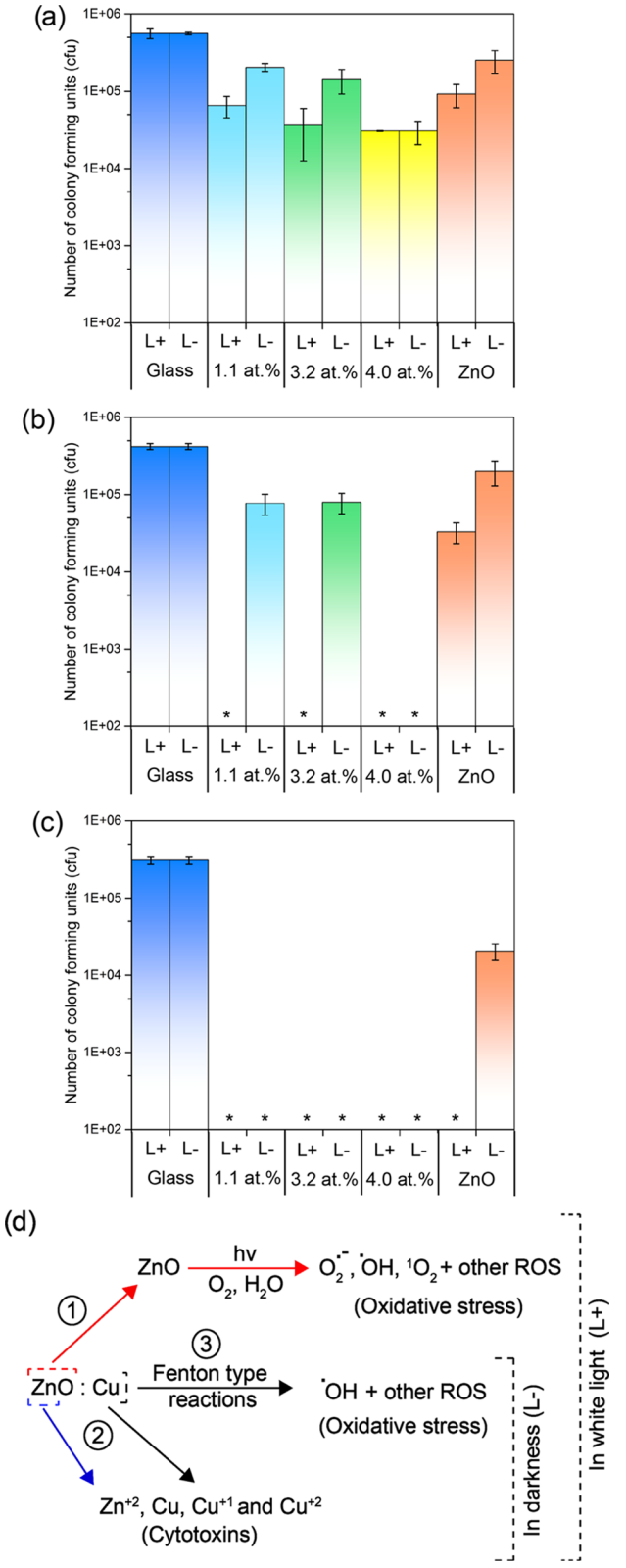

Figure 4. Number of viable colony counts of *E. coli* after incubation on pure and Cu-doped thin films on microscope slides. The number of viable colony counts were determined after (a) 3, (b) 6, and (c) 18 h. L+ = illuminated and L− = not illuminated (in the dark). * Indicates *E. coli* levels below detection limits. (d) Multitude of possible mechanisms via which Cu-doped ZnO is able to disinfect contaminated surfaces. The differing mechanisms of attack that destroy cell membranes, DNA, and proteins of the microbes make the development of resistant strains virtually impossible.

DOI: 10.1021/acsomega.7b00759
ACS Omega 2017, 2, 4556−4562

The increased antimicrobial activity of the Cu-doped films under illumination compared to no illumination is most likely due to a multimechanistic mode of attack. As shown in Figure 4d, it is possible that the light-activated Cu-doped ZnO samples were able to disinfect via three routes: (1) oxidative stress caused by ROS that are produced via reactions between photocatalytically generated electrons/holes and H_2O/O_2, (2) the Zn^{2+}, Cu, Cu^{1+}, and Cu^{2+} ions released from the films that are cytotoxins to microbes above certain concentrations, and (3) ROS species produced via Fenton type reactions that also cause oxidative stress upon microbes. However, in darkness, route 1 is not likely; therefore, only routes 2 and 3 could take place.

Cu-doped samples performed better compared to pure ZnO under both light and dark conditions. Under darkness, this is due to the antimicrobial properties of Cu, but under light conditions, we believe it is due to superior charge carrier lifetimes. One of the mechanisms of action for ZnO, when illuminated with UV radiation above 3.3 eV, is via oxidative stress caused by ROS. These species are produced via redox reactions involving electrons (excited to the conduction band) and holes (remaining in the valence band) on the surface of the ZnO films. The lower the recombination rate the longer the lifetimes of the electron−hole pairs and the higher the chance that these electrons and holes migrate to the surface from the bulk to undergo the redox reactions. In Cu-doped ZnO, the dopant states within the band structure act as trap sites reducing recombination.[46,47] This is common in many metal-doped metal oxide systems and has been experimentally determined using transient absorption spectroscopy.[46] Hence, Cu-doped ZnO samples show increased antimicrobial activity over that of pure ZnO samples under light conditions.

Water Contact Angle Measurements. Evidence that the films are photocatalytically active and route 1 (in Figure 4d) is able to proceed under white light illumination over the time period of the antibacterial testing was determined through water contact angle measurements (Figure 5). Photoinduced wettability in ZnO occurs due to its photosensitivity.[48,49] It takes place when ZnO is activated with light of energy above 3.3 eV, through the migration of photogenerated electrons and holes from the bulk to the surface of the films, similar to route 1 shown in Figure 4d. Some of these holes are thought to react with lattice oxygen to generate oxygen vacancies that are sites for hydroxyl adsorption, which increases surface hydrophilicity and reduces the contact angle between the surface and any water droplet.[48,50]

The pure and Cu-doped films showed a decrease in the water contact angle with increasing irradiation time. As shown is Figure 5b, the greatest decrease was observed for 4.0 atom %, followed by 3.2 atom %, 1.1 atom %, and pure ZnO. This collaborates with what was seen in the antibacterial study and the earlier mentioned idea that the presence of Cu in the ZnO films enhances electron and hole lifetimes thus increasing the probability of them reaching the surface of the films without recombination.

CONCLUSIONS

We demonstrate the novel use of AACVD for the growth of pure ZnO and Cu-doped ZnO thin films. The films were phase pure crystalline matching the hexagonal unit cell of the wurtzite crystal structure. XPS analysis showed Zn in the +2 oxidation state, whereas Cu was in 0 and/or +1 state on the surface. UV−vis spectroscopy shows no significant decrease in the band gap

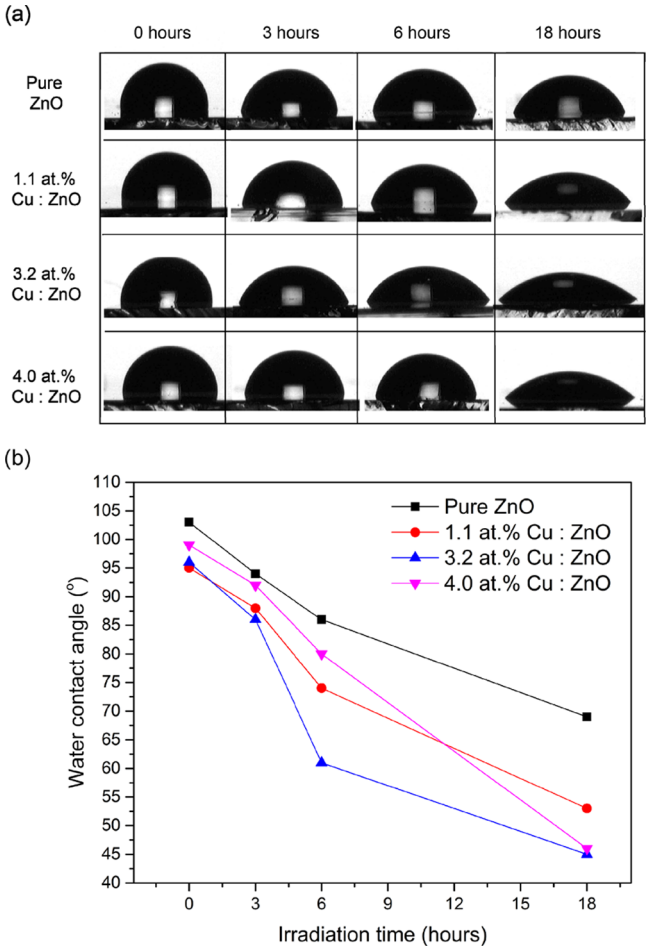

Figure 5. (a) Photographs of the change in water contact angle on the surface of the pure and Cu-doped ZnO films with white light irradiation time and (b) the change in contact angle on the pure and Cu-doped films, as a function of irradiation time.

with increasing Cu concentration in the ZnO matrix, as previously seen for this level of Cu doping. The increased antibacterial activity of the Cu-doped ZnO films compared to that of the pure ZnO films was due to the multiple mechanisms of attack allowed through oxidative stress caused by ROS and cytotoxicity caused by the release of Zn^{2+}, Cu^0, Cu^{1+}, and Cu^{2+} ions. The multiroute to disinfection also avoids the possible risk of bacterial resistance development, a major concern in world health care at present.

EXPERIMENTAL SECTION

All chemicals used in this report were purchased from Sigma-Aldrich Chemical Co. and used as received. Deposition was on microscope slides or 150 × 45 × 45 mm^3 SiO_2 (50 nm)-coated float-glass (the SiO_2 acts as a barrier layer preventing diffusion of ions from within the glass into the deposition film), which has been supplied by Pilkington NSG. Prior to use, the glass substrates were cleaned with water, 2-propanol, and acetone.

Deposition Procedure. Depositions were carried out under N_2 (BOC Ltd., 99.99% purity) flow. Zinc acetate dihydrate ($Zn(OAc)_2{\cdot}2H_2O$) (99%), copper dihydrate ($Cu(OAc){\cdot}2H_2O$) (99%), and methanol (99%) were purchased from Sigma and used as received.

$Zn(OAc)_2{\cdot}2H_2O$ (2.28 mmol) was dissolved in MeOH (30 mL) in a glass bubbler. The resulting solution was stirred for 10

DOI: 10.1021/acsomega.7b00759
ACS Omega 2017, 2, 4556−4562

min and then atomized using a piezoelectric device (Johnson Matthey liquifog). For the Cu-doped ZnO films, $Cu(OAc)\cdot 2H_2O$ (2, 4, and 8 mol % relative to $Zn(OAc)_2\cdot 2H_2O$) was dissolved in methanol (30 mL) in a separate glass bubbler, stirred for 10 min and then atomized. The Zn precursor and Cu precursor flows were both kept at 0.5 L min^{-1}, and the two aerosol flows were mixed at a Y junction and delivered into the cold wall chemical vapor deposition reaction chamber, as shown in the Supporting Information, using the N_2 carrier gas.

The glass substrate (4 mm float glass coated with a SiO_2 barrier layer) temperature was 350 °C, and the deposition time was 60 min. After the deposition, the bubblers were closed and the substrates were cooled under a flow of air. Only the pure ZnO film was cooled under a N_2 flow. The glass substrate was allowed to cool with the graphite block to less than 100 °C before it was removed. Coated substrates were handled and stored in air.

Characterization. Powder X-ray diffraction (PXRD) was carried out using a modified Bruker-Axs D8 diffractometer, with parallel beam optics and a PSD LynxEye silicon strip detector. Unmonochromated Cu Kα source operated at 40 kV with 30 mA emission current was used. The incident beam angle was set at 0.5° and the 2θ range of 10−65° was measured with a step size of 0.05° at 1 s/step.

JEOL JSM-6301F field emission scanning electron microscope (SEM) at an accelerating voltage of 5 keV was used for SEM measurements.

Optical measurements were carried out using a PerkinElmer Fourier transform Lambda 950 spectrometer over a wavelength range of 300−2500 nm.

X-ray photoelectron spectroscopy (XPS) was performed using a Thermo Scientific K-Alpha photoelectron spectrometer using monochromatic Al Kα radiation. Higher resolution scans were recorded for the principal peaks of Cu(2p), Zn(2p), O(1s), and C(1s) at a pass energy of 50 eV. The peaks were modeled using CasaXPS software, with binding energies adjusted to adventitious carbon (284.5 eV) for charge correction.

Antimicrobial Activity. A procedure similar to that of Hassan et al. was used for the antibacterial tastings.[28]

Brain heart infusion (BHI) agar (Oxoid; Basingstoke, U.K.) was used to maintain *E. coli* strain (ATCC 25922) by weekly subculture. Ten milliliters of sterile BHI broth (Oxoid; Basingstoke, U.K.) was inoculated by *E. coli* and incubated aerobically with shaking at 37 °C for 24 h. Bacteria from the overnight culture were collected by centrifugation at 13 000*g* for 1 min. *E. coli* was then resuspended in phosphate-buffered saline (PBS) (Oxoid; Basingstoke, U.K.) and centrifuged at 13 000*g* for 1 min. The bacterial pellet was resuspended in PBS prior to use. The cloudiness of the bacterial cell suspension was measured at 600 nm using a spectrophotometer and was adjusted to an optical density of approximately 10^5 cfu per 25 μL aliquot.

The pure ZnO and Cu-doped ZnO slides were cut into 1 × 1 cm^2 sections. A humidity chamber was used to minimize drying out of the suspensions. A 25 μL aliquot of the bacterial cell suspension was spread on each slide and incubated at room temperature (21 ± 2 °C) for the required exposure time. For each exposure time (3, 6, and 18 h), triplicate samples were analyzed and uncoated glass microscope slides were used as a control. The samples were then irradiated for up to 18 h using a white light source (General Electric 28 W Watt Miser T5 2D compact fluorescent lamp) emitting an average light intensity of 3750 lx at a distance of 30 cm from the samples. A further set of samples (in triplicate) was maintained in the dark for the duration of the irradiation time. Each exposure time was repeated on two separate occasions

Postincubation, the slides were aseptically transferred to a 225 μL PBS and vortexed for 30 s to release the bacteria into the solution. Serial dilutions of the resulting bacterial suspensions were prepared in PBS and 25 μL from each dilution was spread on to MacConkey agar (Oxoid; Basingstoke, U.K.). Plates were incubated aerobically at 37 °C for 24 h. Postincubation, any bacterial colonies formed were counted and the number of viable bacteria was calculated. The Mann−Whitney *U* test was used to determine the significance of the activity of zinc oxide or copper zinc oxide slides compared with the glass control.

Water Contact Angle Measurements. Water droplet contact angles were measured using a First Ten Angstroms 1000 device, with a side-mounted rapid fire camera fire-casting 3 μL droplets from a fixed height onto the surface. Photoinduced wettability was tested by placing the samples under a white light source for 0, 3, 6, and 18 h and then measuring the water contact angle by placing a 3 μL droplet onto the surface of the films.

■ ASSOCIATED CONTENT

Supporting Information

The Supporting Information is available free of charge on the ACS Publications website at DOI: 10.1021/acsomega.7b00759.

Schematic of the AACVD reactor used to grow the pure and Cu-doped ZnO thin films; photograph showing the high transparency of the thin films; EDS results (PDF)

■ AUTHOR INFORMATION

Corresponding Author

*E-mail: c.j.carmalt@ucl.ac.uk. Fax: (+44) 20-7679-7463.

ORCID

Sanjayan Sathasivam: 0000-0002-5206-9558

Claire J. Carmalt: 0000-0003-1788-6971

Author Contributions

I.A.H. synthesized the coatings and carried out the antibacterial characterization. I.A.H. and S.S. performed the material characterization and data analysis. S.S. wrote the article with contributions from I.A.H., C.J.C., and S.P.N. C.J.C. and S.P.N. supervised I.A.H. All authors contributed to scientific discussions throughout the work.

Notes

The authors declare no competing financial interest.

■ ACKNOWLEDGMENTS

The EPSRC are thanked for studentship funding (I.A.H.) through the Molecular Modeling and Materials Science Doctoral Training Center (grant EP/G036675).

■ REFERENCES

(1) Musat, V.; Teixeira, B.; Fortunato, E.; Monteiro, R. C. C.; Vilarinho, P. *Surf. Coat. Technol.* **2004**, *180−181*, 659−662.

(2) Matsubara, K.; Fons, P.; Iwata, K.; Yamada, A.; Sakurai, K.; Tampo, H.; Niki, S. *Thin Solid Films* **2003**, *431−432*, 369−372.

(3) Magill, S. S.; Edwards, J. R.; Bamberg, W.; Beldavs, Z. G.; Dumyati, G.; Kainer, M. A.; Lynfield, R.; Maloney, M.; McAllister-Hollod, L.; Nadle, J.; et al. *N. Engl. J. Med.* **2014**, *370*, 1198−1208.

DOI: 10.1021/acsomega.7b00759
ACS Omega 2017, 2, 4556−4562

(4) Review on Antimicrobial Resistance; Grande-Bretagne *Antimicrobial Resistance: Tackling a Crisis for the Health and Wealth of Nations*; Review on Antimicrobial Resistance, 2014.
(5) Taylor, J.; Hafner, M.; Yerushalmi, E.; Smith, R.; Bellasio, J.; Vardavas, R.; Bienkowska-Gibbs, T.; Rubin, J. *Model and Results*; RAND Corporation: Cambridge, 2014.
(6) Climo, M. W.; Yokoe, D. S.; Warren, D. K.; Perl, T. M.; Bolon, M.; Herwaldt, L. A.; Weinstein, R. A.; Sepkowitz, K. A.; Jernigan, J. A.; Sanogo, K.; Wong, E. S. *N. Engl. J. Med.* **2013**, *368*, 533−542.
(7) Page, K.; Palgrave, R. G.; Parkin, I. P.; Wilson, M.; Savin, S. L. P.; Chadwick, A. V. *J. Mater. Chem.* **2007**, *17*, 95−104.
(8) Neu, H. C. *Science* **1992**, *257*, 1064−1073.
(9) Bovis, M. J.; Noimark, S.; Woodhams, J. H.; Kay, C. W. M.; Weiner, J.; Peveler, W. J.; Correia, A.; Wilson, M.; Allan, E.; Parkin, I. P.; MacRobert, A. J. *RSC Adv.* **2015**, *5*, 54830−54842.
(10) Noimark, S.; Dunnill, C. W.; Kay, C. W. M.; Perni, S.; Prokopovich, P.; Ismail, S.; Wilson, M.; Parkin, I. P. *J. Mater. Chem.* **2012**, *22*, 15388−15396.
(11) Perni, S.; Piccirillo, C.; Pratten, J.; Prokopovich, P.; Chrzanowski, W.; Parkin, I. P.; Wilson, M. *Biomaterials* **2009**, *30*, 89−93.
(12) Xie, Y.; He, Y.; Irwin, P. L.; Jin, T.; Shi, X. *Appl. Environ. Microbiol.* **2011**, *77*, 2325−2331.
(13) Ripa, S.; Ripa, R. *Minerva Med.* **1994**, *86*, 315−318.
(14) Sirelkhatim, A.; Mahmud, S.; Seeni, A.; Kaus, N. H. M.; Ann, L. C.; Bakhori, S. K. M.; Hasan, H.; Mohamad, D. *Nano-Micro Lett.* **2015**, *7*, 219.
(15) Jiang, W.; Mashayekhi, H.; Xing, B. *Environ. Pollut.* **2009**, *157*, 1619−1625.
(16) Brayner, R.; Ferrari-Iliou, R.; Brivois, N.; Djediat, S.; Benedetti, M. F.; Fiévet, F. *Nano Lett.* **2006**, *6*, 866−870.
(17) Jones, N.; Ray, B.; Ranjit, K. T.; Manna, A. C. *FEMS Microbiol. Lett.* **2008**, *279*, 71−76.
(18) Ann, L. C.; Mahmud, S.; Bakhori, S. K. M.; Sirelkhatim, A.; Mohamad, D.; Hasan, H.; Seeni, A.; Rahman, R. A. *Ceram. Int.* **2014**, *40*, 2993−3001.
(19) Gittard, S. D.; Perfect, J. R.; Monteiro-Riviere, N. A.; Wei, W.; Jin, C.; Narayan, R. J. *Appl. Surf. Sci.* **2009**, *255*, 5806−5811.
(20) Carvalho, P.; Sampaio, P.; Azevedo, S.; Vaz, C.; Espinós, J. P.; Teixeira, V.; Carneiro, J. O. *Appl. Surf. Sci.* **2014**, *307*, 548−557.
(21) Cuevas, A. G.; Balangcod, K.; Balangcod, T.; Jasmin, A. *Procedia Eng.* **2013**, *68*, 537−543.
(22) Ozkan, E.; Ozkan, F. T.; Allan, E.; Parkin, I. P. *RSC Adv.* **2015**, *5*, 8806−8813.
(23) Kääriäinen, M.-L.; Weiss, C. K.; Ritz, S.; Pütz, S.; Cameron, D. C.; Mailänder, V.; Landfester, K. *Appl. Surf. Sci.* **2013**, *287*, 375−380.
(24) Li, Y.; Zhang, W.; Niu, J.; Chen, Y. *ACS Nano* **2012**, *6*, 5164−5173.
(25) Xia, T.; Kovochich, M.; Brant, J.; Hotze, M.; Sempf, J.; Oberley, T.; Sioutas, C.; Yeh, J. I.; Wiesner, M. R.; Nel, A. E. *Nano Lett.* **2006**, *6*, 1794−1807.
(26) Xia, T.; Kovochich, M.; Liong, M.; Mädler, L.; Gilbert, B.; Shi, H.; Yeh, J. I.; Zink, J. I.; Nel, A. E. *ACS Nano* **2008**, *2*, 2121−2134.
(27) Burello, E.; Worth, A. P. *Nanotoxicology* **2011**, *5*, 228−235.
(28) Hassan, I. A.; Parkin, I. P.; Nair, S. P.; Carmalt, C. J. *J. Mater. Chem. B* **2014**, *2*, 2855−2860.
(29) Ruparelia, J. P.; Chatterjee, A. K.; Duttagupta, S. P.; Mukherji, S. *Acta Biomater.* **2008**, *4*, 707−716.
(30) Santo, C. E.; Morais, P. V.; Grass, G. *Appl. Environ. Microbiol.* **2010**, *76*, 1341−1348.
(31) Bhachu, D. S.; Sathasivam, S.; Sankar, G.; Scanlon, D. O.; Cibin, G.; Carmalt, C. J.; Parkin, I. P.; Watson, G. W.; Bawaked, S. M.; Obaid, A. Y.; Al-Thabaiti, S.; Basahel, S. N. *Adv. Funct. Mater.* **2014**, *24*, 5075−5085.
(32) Ferhat, M.; Zaoui, A.; Ahuja, R. *Appl. Phys. Lett.* **2009**, *94*, No. 142502.
(33) Bhuyan, T.; Khanuja, M.; Sharma, R.; Patel, S.; Reddy, M. R.; Anand, S.; Varma, A. *J. Nanopart. Res.* **2015**, *17*, 1−11.
(34) Knapp, C. E.; Carmalt, C. J. *Chem. Soc. Rev.* **2016**, *45*, 1036−1064.
(35) Marchand, P.; Hassan, I. A.; Parkin, I. P.; Carmalt, C. J. *Dalton Trans.* **2013**, *42*, 9406−9422.
(36) Sathasivam, S.; Arnepalli, R. R.; Kumar, B.; Singh, K. K.; Visser, R. J.; Blackman, C. S.; Carmalt, C. J. *Chem. Mater.* **2014**, *26*, 4419−4424.
(37) Sathasivam, S.; Bhachu, D. S.; Lu, Y.; Chadwick, N.; Althabaiti, S. A.; Alyoubi, A. O.; Basahel, S. N.; Carmalt, C. J.; Parkin, I. P. *Sci. Rep.* **2015**, *5*, No. 10952.
(38) Bhachu, D. S.; Sathasivam, S.; Carmalt, C. J.; Parkin, I. P. *Langmuir* **2014**, *30*, 624−630.
(39) Bhachu, D. S.; Moniz, S. J. A.; Sathasivam, S.; Scanlon, D. O.; Walsh, A.; Bawaked, S. M.; Mokhtar, M.; Obaid, A. Y.; Parkin, I. P.; Tang, J.; Carmalt, C. J. *Chem. Sci.* **2016**, 4832.
(40) Mittal, K. L. *Act. Passive Electron. Compon.* **1976**, *3*, 21−42.
(41) Ponja, S. D.; Sathasivam, S.; Parkin, I. P.; Carmalt, C. J. *RSC Adv.* **2014**, *4*, 49723−49728.
(42) Waugh, M. R.; Hyett, G.; Parkin, I. P. *Chem. Vap. Deposition* **2008**, *14*, 366−372.
(43) Biesinger, M. C.; Lau, L. W. M.; Gerson, A. R.; Smart, R. S. C. *Appl. Surf. Sci.* **2010**, *257*, 887−898.
(44) Deroubaix, G.; Marcus, P. *Surf. Interface Anal.* **1992**, *18*, 39−46.
(45) Girard, R. T.; Tjernberg, O.; Chiaia, G.; Söderholm, S.; Karlsson, U. O.; Wigren, C.; Nylén, H.; Lindau, I. *Surf. Sci.* **1997**, *373*, 409−417.
(46) Choi, W.; Termin, A.; Hoffmann, M. R. *J. Phys. Chem.* **1994**, *98*, 13669−13679.
(47) Jaimy, K. B.; Safeena, V. P.; Ghosh, S.; Hebalkar, N. Y.; Warrier, K. G. K. *Dalton Trans.* **2012**, *41*, 4824−4832.
(48) Sun, R.-D.; Nakajima, A.; Fujishima, A.; Watanabe, T.; Hashimoto, K. *J. Phys. Chem. B* **2001**, *105*, 1984−1990.
(49) Feng, X.; Feng, L.; Jin, M.; Zhai, J.; Jiang, L.; Zhu, D. *J. Am. Chem. Soc.* **2004**, *126*, 62−63.
(50) Kenanakis, G.; Stratakis, E.; Vlachou, K.; Vernardou, D.; Koudoumas, E.; Katsarakis, N. *Appl. Surf. Sci.* **2008**, *254*, 5695−5699.

DOI: 10.1021/acsomega.7b00759
ACS Omega 2017, 2, 4556−4562